# 1GHz loop antennas based smart contact lenses

Patrice Salzenstein [1], Aya Maroua Bessou [1], Laurine Salzenstein [2]
[1] Centre National de la Recherche Scientifique (CNRS), Université Marie et Louis Pasteur (UMLP), FEMTO-ST Institute, 15B avenue des Montboucons, F25030 Besançon Cedex, FRANCE
[2] Université Marie et Louis Pasteur (UMLP), Information Technology (IT) DEpartment, F25000 Besançon Cedex, FRANCE
***e-mail:*** *patrice.salzenstein@cnrs.fr , bessouayamaroua@gmail.com , laurine.salzenstein@gmail.com*

## ABSTRACT

This work investigates the electromagnetic design, performance, and thermal aspects of microfabricated double-loop antennas for self-powered smart contact lenses. A compact stacked double-loop structure with 9.5 mm diameter loops is optimized for 900 MHz–1.1 GHz, resonating near 1.01 GHz. The antenna produces a broad radiation pattern with preferred vertical directions (θ = 0° and 180°), enabling wireless communication with devices like smartphones and smartwatches. Its Q-factor of ~5 ensures wideband operation while fitting strict lens size constraints. Electrical and thermal analyses reveal resistive losses due to skin effect in gold conductors, with a skin depth of ~0.7 µm leading to low radiation efficiency (0.02–0.71%). Coupling between large and small loops (k ≈ 0.59) supports near-field sensing and wireless power transfer. Despite radiation limitations, these antennas show strong potential for reliable short-range communication in autonomous, biocompatible smart contact lenses.

**Keywords:** lens, eye, energy, optics, antenna, 1GHz.

## 1. INTRODUCTION

After an investigation in designing smart contact lenses [1, 2], this work focuses on the electromagnetic design, performance analysis, and thermal considerations of microfabricated double-loop antennas specifically developed for self-powered smart contact lenses. In a first part, we present a compact stacked double-loop antenna structure, consisting of two vertically aligned loops with a diameter of 9.5 mm, optimized for directional radiation in the 900 MHz to 1.1 GHz frequency range. The resonant frequency, estimated using small loop antenna theory, is centred at approximately 1.01 GHz. The antenna exhibits a broad radiation pattern with preferred emission and reception directions along the vertical axis (θ = 0° and θ = 180°), making it suitable for wireless communication with external devices such as smartphones and smartwatches. The calculated Q-factor of approximately 5 ensures wideband operation, while maintaining efficient signal transfer within the strict spatial constraints of a contact lens. The second part extends this analysis by addressing the electrical and thermal performance of the antenna. Using gold as the conductor material, the study quantifies resistive losses induced by skin effect, given the small wire dimensions and high operational frequency. The skin depth is calculated at approximately 0.7 µm, indicating dominant current conduction near the wire surface, which contributes to significant resistive losses and low radiation efficiency (0.02-0.71%). Furthermore, mutual inductance and coupling coefficients between the large and small loops are assessed, confirming moderate inductive coupling (k ≈ 0.59) suitable for near-field sensing and wireless power transfer. The integration of these antennas into smart contact lenses demonstrates their potential for reliable, short-range communication despite inherent radiation limitations, marking a significant advancement in the development of autonomous, biocompatible wearable biomedical devices.

## 2. OPERATING FREQUENCY RANGE

This section presents the technical characteristics of a compact stacked double loop antenna designed for directional electromagnetic transmission and reception. The loop antenna or magnetic loop antenna is sensitive to the magnetic field (hence its name magnetic loop). Its general operating principle results from a direct application of the Lenz-Faraday law, the induced voltage being proportional to the flux of the magnetic field, the loop antenna belongs to the category of fluxmeters.

The structure comprises two vertically aligned circular loops, which function collectively as magnetic dipoles. Such a configuration enhances directional radiation, making it suitable for applications requiring focused signal propagation or sensing. The antenna has a loop diameter of 9.5 mm. It is chosen to stay compatible with typical dimensions of lenses and without masking the vision. We will see that it corresponds to a resonant frequency near 1.01 GHz, based on established principles of small loop antenna theory. The effective operating frequency range spans from 900 MHz to 1.1 GHz, covering a bandwidth appropriate for many modern communication and detection systems. The antenna's radiation pattern is optimized along the vertical axis (broadside to the loop plane), where emission and reception are strongest at angles $\theta = 0°$ and $\theta = 180°$. This directionality improves signal gain and precision in targeted scenarios. This section outlines the relevant physical parameters, theoretical calculations, and practical considerations including the use of the speed of light in estimating frequency and wavelength. This analysis contributes to a broader understanding of antenna performance, design constraints, and application-specific deployment within the specified GHz range.

*2.1. Antenna Structure, Dimensions, Range and Resonant Frequency*

A stacked double loop antenna consists of two circular loops aligned vertically, functioning as magnetic dipoles. This structure is often used for directional emission and reception, behaving like two magnetic dipoles in phase. These antennas are used for directional radiation and reception. For a loop with a 9.5 mm diameter ($D = 0.0095$ m), the radius is $r = D / 2 = 4.75$ mm, leading to a loop circumference of approximately $C = 2\pi r = 0.0298$ m. In small loop antenna theory, resonance typically occurs when the circumference is about one-tenth of the wavelength. Thus, the estimated resonant wavelength is 0.298 m. For small loop antennas, the resonant condition typically occurs when the loop circumference is approximately 1/10 of the wavelength ($\lambda$). We assume that the loop diameter is $D = 9.5$ mm. The key criterion for a small loop antenna is: loop circumference C is negligible compared to $\lambda$ with $\frac{c}{\lambda} < \frac{1}{10}$ (*Equation 1).* Using those formula: $\lambda \approx 10 \times C = 0.298$ m *(Equation 2)*, $f = c / \lambda \approx 3 \times 10^8 / 0.298 \approx 1.01$ GHz *(Equation 3),* and using the speed of light ($c = 3 \times 10^8$ m/s), the resonant frequency is approximately determined as 1.01 GHz. Given a centered resonant frequency of ~1.01 GHz, the typical usable bandwidth is approximately 900 MHz to 1.1 GHz. Since antennas are reciprocal, they operate similarly for both transmission and reception, that's why the expected operating frequency range for this antenna is in [900 MHz, 1.1 GHz]. The exact usable bandwidth may vary depending on the antenna's Q-factor and matching components. Since antennas are reciprocal, the operating frequency range is the same for both transmission and reception. Given a centered resonant frequency of ~1.01 GHz, the typical usable bandwidth is approximately 900 MHz to 1.1 GHz.

*2.2. First approach for directional properties, preferred angles and Q-factor*

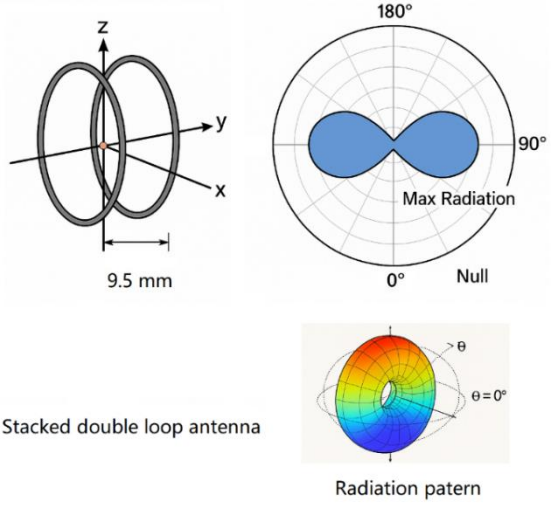


**Figure 1.** Small double loop antenna of 9.5 mm diameter, real distances between antenna are not respected to enable a better representation. Radiation of a small loop antenna is donut-shaped like a magnetic dipole. Maximum radiation is in the plane of the loop. Color for illustration purpose. Null – or Zero radiation, is along the axis perpendicular to the loop plane. For small loops, radiation resistance $Rr = 20\pi^2 \times (A/\lambda^2)^2$ where $A = \pi r^2$ is the area of the loop and $\lambda = c/f$.

Figure1 gives the small double loop antenna of 9.5 mm diameter main characteristics. The radiation pattern of a single loop is Donut-shaped with maximum emission perpendicular to the plane of the loop. However, in a stacked configuration, the pattern becomes more directional, with maximum radiation occurring along the vertical axis (broadside), i.e., at $\theta = 0°$ and $\theta = 180°$ relative to loop plane.

So preferred emission/reception directions are along the axis of the loop stack: θ = 0° and θ = 180°. This improves directivity and gain in those directions, making the antenna more effective for targeted communication or sensing. When two such loops are stacked, the radiation is reinforced along the axis of the loop stack. Single loop antenna radiates most strongly in the plane perpendicular to its axis. The Q-factor (quality factor) of a small loop antenna is typically estimated as

$$\boldsymbol{Q} \approx \frac{\boldsymbol{f_0}}{\boldsymbol{\Delta f}} \quad \textit{(Equation 4)}$$

Given f0 = 1.01 GHz and $\Delta$ f = 200 MHz (-3 dB bandwidth), the estimated Q-factor is approximately as $\boldsymbol{Q} \approx \frac{\boldsymbol{1010}}{\boldsymbol{200}}$. It gives Q ≈ 5.05. This is very low, which is favorable for wideband operation and suggests the antenna is efficient for communication. We can also roughly estimate the theoretical Q-factor of a small loop antenna using the radiation resistance Rr and loss resistance Rl:

$$Q = \frac{2\pi \mathrm{f} \mathrm{L}}{R} \quad (Equation\ 5)$$

However, this requires an estimation of the inductance L of the loop, and knowing or approximating the resistance R. For a single-turn circular loop of radius r, made from a thin conductor, inductance of the loop is:

$$L = \mu_0 \mathrm{r}\left[Ln\left(\frac{8\mathrm{r}}{\mathrm{a}}\right) - 2\right] \quad (Equation\ 6)$$

where r=4.75 mm, wire radius could be a=25 μm, and μ0 = 4π×10−7 H/m. Using this, we can say the inductance is in the nH range, and combined with expected loss resistance of several ohms, a Q-factor of 5 to 10 maximum is typical and reasonable for such compact antennas. It gives L=5.96nH.

*2.3. Discussion*

Uncertainty has to be systematically estimated as we already discuss in [3–9] and it is important to underline that with such system typically operating from 900 MHz to 1.1 GHz. The upper limit of 1.1 GHz is the physical limit for small loop behavior for 9.5 mm loops. This frequency range is compatible with control operated by compact and portable circuits. In this section we summarize the main parameters for the operating frequency range and direction of antennas. They are given in Table 1. These settings are perfectly compatible with transmission to a portable device such as a smartwatch or smartphone.

**Table 1.** Settings for the operating frequency range and direction of antennas.

| Parameter | Determination | Value – Range |
|---|---|---|
| Operating Frequency[1] | Tx/Rx | 900 MHz – 1.1 GHz |
| Resonant Frequency Estimation | f = c / λ | 1.01 GHz |
| Preferred Radiation Angles | | 0° – 180° |

[1] Wavelength estimation: λ ≈ 10C with small loop approximation. Estimated operational bandwidth is given at -3dB.

## 3. ELECTRICAL AND THERMAL EFFECTS OF ANTENNAS

The polar plot given in Figure 2 shows the normalized radiation pattern of the loop antenna in the far-field. It's a typical donut-shaped (toroidal) pattern characteristic of small loop antennas, with maximum radiation perpendicular to the plane of the loop and nulls along the axis. Classic small loop pattern proportional to $\sin^2(\theta)$, indicating nulls along the axis of the loop and maximums in the plane of the loop. Radiation pattern of the small loop antenna, showing the classic toroidal shape (donut-like structure) where radiation is strongest in the plane of the loop and nulls occur along the axis perpendicular to the plane.

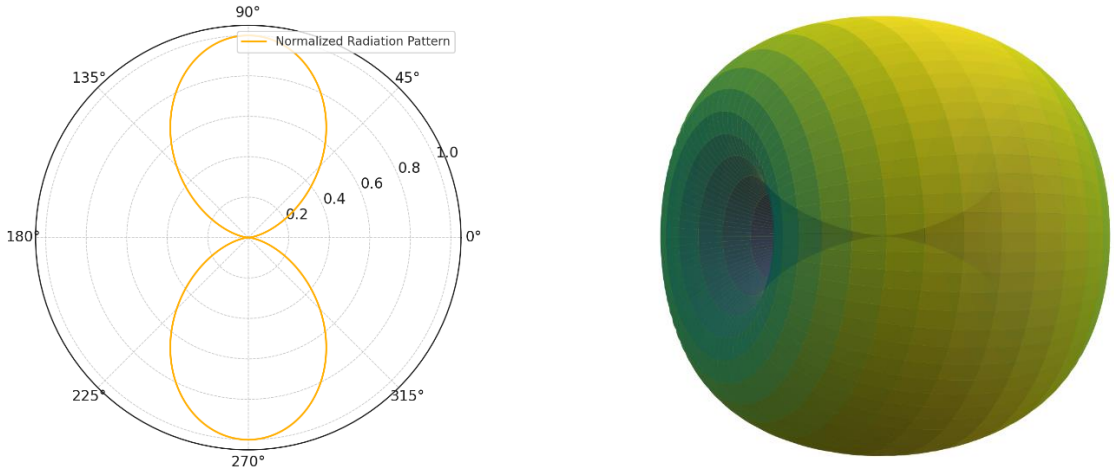


(a) (b)

**Figure 2.** (a) Small double loop antenna of 9.5 mm diameter normalized radiation pattern. (b) 3D radiation pattern.

Antenna Geometry Overview: we draw inspiration from the results of F. Callias' work on magnetic loop antennas and microtechnology in general [10]. In reference [11], F. Callias, offers a comprehensive examination of shortwave loop antennas, focusing on their design, theoretical foundations, and practical applications. It encompasses calculations for transmission balance in free space, impedance considerations for transmitting loop antennas, noise factors affecting shortwave reception, and provides detailed guidance on constructing both passive and active wideband receiving loop antennas. Small microwave loop antenna is studied accordingly to K. Siwiak's papers.

**Table 2.** Settings for parameters of antennas[1].

| Parameter | Designation | Value (Range) |
|---|---|---|
| Hydrogel contact lens diameter | $D_L$ | 10 mm |
| Radius of large loop antenna | $r_1$ | 4.75 mm |
| Radius of smaller loop antenna | $r_2$ | 0.95 mm |
| Wire thickness | 2a | 50 μm |
| Wire radius | a | 25 μm |
| Large loop antenna area | $A_1$ | $7.09\times10^{-5}$ m² |
| Smaller loop antenna area | $A_2$ | $2.83\times10^{-6}$ m² |
| Thermal conductivity of Gold | κ | 318 W/mK |
| Electrical resistivity of Gold | ϱ | $2.44\times10^{-8}$ Ω·m |
| Electrical conductivity of Gold | $\sigma_{Au}$ | $4.52\times10^{7}$ S/m |
| Electrical conductivity of Hydrogel | $\sigma_H$ | 0.3 S/m |
| Relative permittivity of Hydrogel in 900 – 1100 MHz range GHz | $E_H$ | 79 |
| Vacuum permeability | $\mu_0$ | $4\pi\times10^{-7}$ H/m |

[1] References for parameters of Gold [12] and Hydrogel [13-15].

Efficiency and frequency bandwidth are given in Figure 3 accordingly. References [16] and [17] provide foundational analyses of the near-field and radiation characteristics of annular antennas, offering insights into their performance in vehicular applications. Reference [18] by Siwiak and Rohde extends this knowledge by discussing practical tuning techniques for electrically short antennas, crucial for optimizing loop antenna performance in field conditions. Lastly, reference [19] explores minimum coupling antenna arrays, presenting methods to reduce mutual interference in multi-antenna systems, which is highly relevant for compact loop antenna deployments in modern communication environments.

Reference [20] gives a dipole antenna design that achieves ultra-wideband performance with improved impedance matching and compact size. According to those studies of K. Siwiak, we provide our results concerning the loop antenna. Reference [21] presents a novel nonuniform loop antenna design optimized for C-band applications, demonstrating enhanced bandwidth and radiation characteristics compared to traditional uniform loop antennas. Metal is deposited on the lens as in [22].

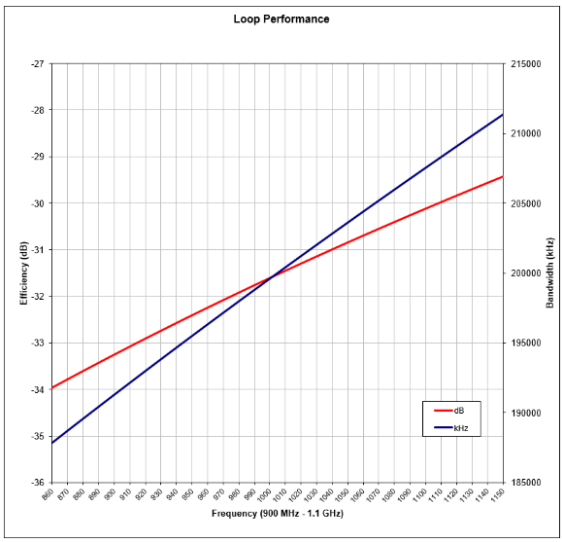


**Figure 3.** Efficiency (in dB) and frequency bandwidth (expressed in kHz) of the main loop antenna versus frequency expressed in MHz is determined according to the 1.01 GHz centered frequency, 9.5 mm diameter, Gold electrical parameters – see Table 2, and based on the work of. Q-factor is predicted at 5.05 and measured at 4.98.

Loop antennas can be analyzed as magnetic dipoles at these sizes (loop << wavelength). The mutual coupling (inductive) depends on distance and orientation, loop areas, relative position (offset vs. concentric) and mutual inductance M. The coupling coefficient k is given by

$$k = \frac{M}{\sqrt{L_1 L_2}} \quad (Equation\ 7)$$

where M is the mutual inductance and $L_1$, $L_2$ are respectively self-inductances of the large and small loops. Self-inductances are estimated as for small single-turn circular loops as in equation 6 relatively to r is the loop radius, a is the wire radius (25 μm) and μ0=4π×10−7 H/m. So, for the larger loop, $L_1 = 5.96$ nH, and for the smaller loop, $L_2 = 4.68$ nH. The coupling coefficient with equation 7 gives k = 0.2. This is moderate to strong coupling, but less than if they were concentric. Results for self-inductances are given in Table 3. Mutual Inductance M can be determined as follow. If the loops were coaxial and centered, we could approximate M using $M = \frac{\mu_0 \cdot (A_1 A_2)}{2\pi \times d^3}$ $(Equation\ 8)$. But since the small loop is placed at the bottom edge of the large loop, mutual coupling is reduced due to non-concentricity. Let's model the reduction using a simplified geometric factor γ, where: $M_{offset} \approx \gamma \cdot M_{centered}$ (*Equation 9*). Typically, for close proximity but off-centered configurations, γ≈0.3−0.5 depending on distance, we keep the value γ≈0.4. Assuming $A_2 = \pi . r^2 = 2.83.10^{-6} m^2$ and distance between centers d≈$r_1$−$r_2$=3.8 mm, then M= γ ·4π×$10^{-7}$·[(7.09×$10^{-5}$ x 2.83×$10^{-6}$)/(2π×0.0033³).

**Table 3.** Calculated parameters[1].

| Parameter | Designation | Value (Range) |
|---|---|---|
| Centered frequency[1] | $F_0$ | 1.01 GHz (900 MHz – 1.1 GHz) |
| Wavelength[1] | λ | 0.297 m |
| Self-Inductance of large loop antenna | $L_1$ | 5.96nH |
| Self-Inductance of smaller loop antenna | $L_2$ | 4.68nH |
| Simplified geometric factor | γ | 0.4 |
| Mutual inductance | M | 0.42nH |
| Coupling Coefficient | k | 0.59 |
| Skin depth | δ | 0.7 μm |
| Large loop antenna area | $A_1$ | 7.09×$10^{-5}$ m² |
| Smaller loop antenna area | $A_2$ | 2.83×$10^{-6}$ m² |
| Radiation resistance | $R_r$ | 0.127 mΩ |
| Radiation efficiency | η | 0.020 – 0.71% |

[1] See part 2 – Operating frequency range.

It gives for the Mutual Inductance: M=0.42nH, reported in Table 3.

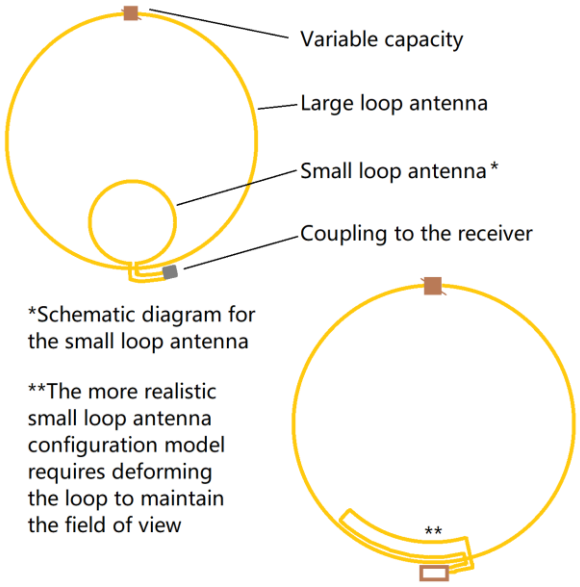


**Figure 4.** This figure illustrates the problem of coupling to the transmitter-receiver antenna with the need to maintain the field of vision through the lens. Gold loops of the antennas are shown in yellow gold color. The brown rectangle in the lower right corner symbolizes the ASIC.

As illustrated on Figure 4, in reality, we need to extract the microwave signal received by this receiving loop antenna. The classic method is to use inductive coupling, as in transmitting. Optimal coupling (not too tight) allows maximum energy to be extracted. Coupling that is "tighter" than optimal dampens the loop by reducing its gain, selectivity, and quality factor. This is acceptable for shortwave reception because the noise received by the antenna is significantly louder than thermal noise. Variable capacity is to fit the resonance of the larger loop antenna around 1.01 GHz. One of the advantages of this configuration is the following. The output level is not very variable in terms of power between 900 MHz and 1.1 GHz, and the quality factor is not very high, since it is around 5. This means that in practice we will avoid having to adjust the variable capacity all the time after adaptation. Such parameters could be specified in further work. Thermal and Resistive Effects are determined considering materials. Gold is a good conductor, but the antennas are very small, so skin effect and resistive losses are still important at 1.01 GHz. Information concerning skin depth is given in Table 3. Skin depth is $\delta = \sqrt{\frac{2\rho}{\mu 0 \cdot \omega}} = 0.7 \mu m$ (*Equation* 10). So, most current is in outer ~1 μm of wire. δ >> 50 μm, so skin effect is dominant. Effective resistance R increases due to small cross-sectional area and skin effect. This system is highly lossy, and mostly near-field reactive coupling dominates. Coupling coefficient is moderate (~0.59), but effective power transfer is severely limited by losses. Mutual inductance is still appreciable given proximity and loop areas. Radiation from either loop is minimal due to poor radiation efficiency. The off-center small loop decreases M, but not drastically - still strong inductive link. The dominant interaction is near-field magnetic coupling, not far-field radiation. We can summarize the main points. The electromagnetic coupling between these two loops is moderately strong inductively. Offset positioning at the bottom weakens but does not nullify the mutual inductance. Power transfer or re-radiation is heavily limited due to (i) Small loop sizes (<< λ), (ii) High conductor losses (tiny gold wires, high resistivity at GHz with skin effect), (iii) Very low radiation resistance. This system is suitable for near-field sensing, mutual inductance-based energy transfer, or implantable communication, but not efficient RF transmission. We assume that a smartwatch could be at 80 cm from the antenna and try to estimate the power of the received signal. The double-loop antenna integrated in the smart contact lens operates around 1 GHz and radiates preferentially along the vertical axis (θ = 0° and 180°), which in principle enables transmission toward a smartwatch positioned about 80 cm away in the same plane. However, this situation is not ideal, since the radiation null of a small loop lies in its plane, meaning that if the watch is not aligned with the vertical radiation lobes, coupling will be very weak. At 80 cm, the separation corresponds to ~2.7 wavelengths ( $\lambda \approx 0.3$ m), which is in the radiating (far-field) zone for such a small loop. Given the very low radiation efficiency of the lens antenna ( $\eta \approx 0.02 - 0.71\%$) [23] and its extremely low radiation resistance (Rr $\approx 0.127$ mΩ), the radiated power is several tens of dB lower than the input power delivered by the ASIC. For instance, if the ASIC drives 0 dBm (1 mW) into the antenna, only about 200 nW to 7 μW is actually radiated. The free-space path loss at 1 GHz over 0.8 m is roughly 30 dB, meaning the received signal power at the smartwatch antenna would drop to the range of –90 dBm to –70 dBm depending on efficiency and orientation. While this level could still be detectable with a sensitive receiver, it

is close to the limit for robust communication. Potential problems include: strong dependence on antenna orientation (since the smartwatch antenna must be aligned with the vertical radiation lobes), absorption [24] and detuning by the lossy hydrogel and the eye tissue, and high resistive losses due to the skin effect in thin gold conductors. These factors suggest that while communication over 80 cm is possible, in practice the link budget is marginal and would require careful optimization of antenna matching, smartwatch sensitivity, and possibly near-field inductive coupling for shorter, more reliable communication. To enhance the communication between a smart contact lens and a smartwatch, several optimization strategies can be employed, focusing on antenna matching, receiver sensitivity, and near-field inductive coupling:

1. Antenna Matching and Efficiency [25]. Improving the radiation efficiency of the lens antenna is crucial. Implementing adaptive matching networks can compensate for detuning effects caused by the surrounding environment, such as the eye's tissue. Additionally, utilizing high-conductivity materials and optimizing antenna geometry can reduce resistive losses and enhance radiation resistance. For instance, integrating high-impedance surfaces has been shown to improve impedance matching in wearable antennas.
2. Smartwatch Receiver Sensitivity [26]. Enhancing the receiver sensitivity of the smartwatch involves improving antenna design to minimize wrist effects and optimizing the front-end electronics to reduce noise figure. A compact, low-profile dual-band wearable textile antenna has been proposed to address these challenges, achieving high gain and efficiency.
3. Near-Field Inductive Coupling [27]. For short-range communication, near-field inductive coupling can be more efficient than radiative methods. Designing integrated couplers that combine near-field communication with wireless power transfer can enhance communication reliability. Such integrated designs have been explored for mobile device applications.
4. Comprehensive System Optimization [28]. A holistic approach involves optimizing both the lens and smartwatch components. This includes designing antennas with high efficiency and appropriate radiation patterns, improving receiver sensitivity, and considering the integration of near-field communication technologies. Recent advancements in wearable antennas based on nanomaterials offer promising avenues for such optimizations.

## 4. CONCLUSION

These developments are further enhanced by integrating compact, low-profile antennas that operate efficiently within the 900 MHz to 1.1 GHz frequency range, enabling secure wireless communication with external devices like smartphones or smartwatches. With a 9.5 mm diameter, this antenna fits the geometry of a soft contact lens and ensures efficient directional transmission toward portable devices such as smartphones and smartwatches. The proposed antenna design maximizes radiation efficiency along preferred vertical axes ($\theta = 0°$ and $\theta = 180°$), and exhibits a low Q-factor (~5), supporting wideband data transmission while fitting comfortably within the spatial limits of a soft contact lens. These characteristics are essential for enabling bidirectional communication. We have highlighted the importance of materials science, especially the role of biocompatible polymers such as PDMS, and advanced fabrication techniques including 3D printing and microfabrication. The integration of antennas, sensors, and ASICs into a lens with a 10 mm diameter requires not only technical precision but also careful consideration of thermal, mechanical, and electromagnetic effects. Antenna modelling and analysis provide evidence that small double - loop designs can achieve reliable near-field communication despite their inherently low radiation efficiency. Our prior work in metrology and optics provided a foundation for evaluating these performance metrics, including modelling noise, intermodulation effects, and thermal stability in microelectronic subsystems. The pathway toward viable, self-powered smart lenses is becoming clearer. The integration of bioenergy sources, compact RF systems, and adaptive optical materials suggests exciting potential for applications in health monitoring, vision enhancement, and real-time user interaction. Continued interdisciplinary collaboration is a key to transforming these prototypes into safe, and functional devices.

## REFERENCES

[1] M.V. Pogurmirskiy, M. Comte, A. Ali, P. Salzenstein, "Investigation into Feasibility of Lens with Miniaturization of Materials and Power Supply," Proc. of SPIE 13524, 135240D (2025). https://doi.org/10.1117/12.3058758.

[2] P. Salzenstein, B. Guichardaz, A.M. Bessou, E. Pavlyuchenko, M. Comte, M.V. Pogumirsky, "Self-Powered Smart Contact Lenses:

A Multidisciplinary Approach to Micro-Scale Energy and 900 MHz–1.1 GHz Bandwidth Microfabricated Loop Antennas Communication Systems," arXiv 2025, arXiv:2505.15593. https://doi.org/10.48550/arXiv.2505.15593.
[3] Salzenstein P., Pavlyuchenko E., Hmima A., Cholley N., Zarubin M., Galliou S., Chembo Y.K., Larger L., " Estimation of the uncertainty for a phase noise optoelectronic metrology system," Physica Scripta T 149, 014025. http://dx.doi.org/10.1088/0031-8949/2012/T149/014025.
[4] Pavlyuchenko E., Salzenstein P., "Application of modern method of calculating uncertainty to microwaves and opto-electronics," Laser Optics 2014 International Conference, Saint Petersburg, Russia, 30 June–4 July 2014. https://doi.org/10.1109/LO.2014.6886449.
[5] Salzenstein P., Wu T.Y., "Uncertainty analysis for a phase-detector based phase noise measurement system," Measurement 85, 118–123 (2016). https://doi.org/10.1016/j.measurement.2016.02.026.
[6] Salzenstein P., Pavlyuchenko E., "Uncertainty Evaluation on a 10.52 GHz (5 dBm) Optoelectronic Oscillator Phase Noise Performance," Micromachines 12(5), 474 (2021). http://dx.doi.org/10.3390/mi12050474
[7] Salzenstein P., Wu T. Y., "Uncertainty estimation for the Brillouin frequency shift measurement using a scanning tandem Fabry-Pérot interferometer," Micromachines 14(7), 1429 (2023). https://doi.org/10.3390/mi14071429
[8] Salzenstein P., Tavernier H., Volyanskiy K., Kim N. N. T., Larger L. and Rubiola E., "Optical mini-disk resonator integrated into a compact optoelectronic oscillator," Acta Physica Polonica A 116(4), 661-663 (2009). http://dx.doi.org/10.12693/APhysPolA.116.661.
[9] Salzenstein P., Cholley N., Kuna A., Abbé P., Lardet-Vieudrin F., Sojdr L. and Chauvin J., "Distributed amplified ultra-stable signal quartz oscillator based," Measurement 45(7), 1937–1939 (2012). https://doi.org/10.1016/j.measurement.2012.03.035.
[10] A. El-Hoiydi, F. Callias, Y. Oesch, C. Kuratli, and R. Kvacek, "18.1 A 1V 3mA 2.4GHz wireless digital audio communication SoC for hearing-aid applications in 0.18µm CMOS," Proc. IEEE Int. Solid-State Circuits Conf. (ISSCC), San Francisco, CA, USA, pp. 310–311, 9–13 Feb. 2014, https://doi.org/10.1109/ISSCC.2014.6757447.
[11] F. Callias, Antennes LOOP ondes courtes: formules de calcul et application à une antenne de réception, Tech. Memo TM051110, Version 1.0, HB9WW, Fontaines, Switzerland (2006). https://hb9ww.org/wp-content/uploads/2013/03/2005_Antennes_LOOP_HB9BLF.pdf (accessed on 29 August June 2025).
[12] Bell, T. Electrical Conductivity of Metals. ThoughtCo 2025, May 8. https://www.thoughtco.com/electrical-conductivity-in-metals-2340117 (accessed on 29 August June 2025).
[13] Pissis P., Kyritsis A., "Electrical conductivity studies in hydrogels," Solid State Ionics 97, 105–113 (1997). https://doi.org/10.1016/S0167-2738(97)00074-X.
[14] Gómez-Galván F., Lara-Ceniceros T., Mercado-Uribe H., "Device for simultaneous measurements of the optical and dielectric properties of hydrogels," Meas. Sci. Technol. 23, 025602 (2012). https://doi.org/10.1088/0957-0233/23/2/025602.
[15] Zhao P., Chen T., Si J., Shi H., Hou X., "Fabrication of a flexible stretchable hydrogel-based antenna using a femtosecond laser for miniaturization," Opt. Express 31, 32704–32716 (2023). https://doi.org/10.1364/OE.496360.
[16] Q. Balzano and K. Siwiak, "The near field of annular antennas," IEEE Trans. Veh. Technol. 36, 173–183 (1987), https://doi.org/10.1109/T-VT.1987.2411668.
[17] Q. Balzano and K. Siwiak, "Radiation from annular antennas," Proc. 36th IEEE Veh. Technol. Conf., Dallas, TX, USA, pp. 15–25 (1986), https://doi.org/10.1109/VTC.1986.1623405.
[18] K. Siwiak and U. L. Rohde, "Tuning electrically short antennas for field operation," Microwave J., pp. 104–126, 14 May 2019, https://www.microwavejournal.com/articles/32231-tuning-electrically-short-antennas-for-field-operation (accessed on 5 June 2025).
[19] Schantz, H. G., Fluhler, J. D., Siwiak, K., & Shoemaker, G. T. Minimum Coupling Antenna Arrays. 2015 Antenna Applications Symposium, Allerton Park, Monticello, IL, USA. https://www.researchgate.net/profile/Hans-Schantz/publication/325908170_Minimum_Coupling_Antenna_Arrays/links/5b2becd14585150d23c1a262/Minimum-Coupling-Antenna-Arrays.pdf (accessed on 29 August June 2025).
[20] Lule E., Babi T., Siwiak K., "Diamond Dipole Antenna for Ultra-Wideband Communications," Microw. Opt. Technol. Lett. 46, 512–514 (2005). https://doi.org/10.1002/mop.21040.
[21] Shastri S.P., Singh R.R., Ajetrao K.V., "Nonuniform C-Band Loop Antenna," Eng. Technol. Appl. Sci. Res. 8, 3496–3501 (2018). https://doi.org/10.48084/etasr.2308.
[22] Salzenstein P., Dupuis O., Helal M., Lheurette E., Vanbésien O., Mounaix P., Lippens D., "Coplanar waveguides on dielectric membranes micromachined on GaAs substrate," Electronics Letters 32(9), 821-822 (1996). http://dx.doi.org/10.1049/el:19960564.
[23] Pfeiffer C., "Fundamental Efficiency Limits for Small Metallic Antennas," IEEE Transactions on Antennas and Propagation 65(4), 1642-1650 (2017). https://doi.org/10.1109/TAP.2017.2670532.
[24] Atanasova G., Atanasov N., "Small Antennas for Wearable Sensor Networks," Sensors 20(18), 5157 (2020). https://doi.org/10.3390/s20174937.
[25] Bait-Suwailam MM, I. Labiano I, Alomainy A. Impedance Enhancement of Textile Grounded Loop Antenna Using High-Impedance Surface (HIS) for Healthcare Applications. Sensors. 2020; 20(14):3809. https://doi.org/10.3390/s20143809.
[26] Sharma, D., Kumar, S., Tiwari, R.N. et al. On body and off body communication using a compact wideband and high gain wearable textile antenna. Sci Rep 14, 14493 (2024). https://doi.org/10.1038/s41598-024-64932-6.
[27] Bae H, Park S. Design of an Integrated Near-Field Communication and Wireless Power Transfer Coupler for Mobile Device Applications. Technologies. 2025; 13(5):207. https://doi.org/10.3390/technologies13050207.
[28] Wang C, Zhang N, Liu C, Ma B, Zhang K, Li R, Wang Q, Zhang S. New Advances in Antenna Design toward Wearable Devices Based on Nanomaterials. Biosensors. 2024; 14(1):35. https://doi.org/10.3390/bios14010035.